Studying boundary layer methane isotopy and vertical mixing processes at a rewetted peatland site by unmanned aircraft system

Astrid Lampert[1], Falk Pätzold[1], Magnus O. Asmussen[1], Lennart Lobitz[1], Thomas Krüger[1], Thomas Rausch[1], Torsten Sachs[1,2], Christian Wille[2], and Ellen Damm[3]

[1]TU Braunschweig, Institute of Flight Guidance, Hermann-Blenk-Str. 27, 38108 Braunschweig, Germany
[2]German Research Centre for Geosciences, Telegrafenberg, 14473 Potsdam, Germany
[3]Alfred Wegener Institute, Helmholtz Centre for Polar and Marine Research, Am Handelshafen 12, 27570 Bremerhaven, Germany

Correspondence: Astrid Lampert (Astrid.Lampert@tu-braunschweig.de)

Abstract.

A proof of concept study was performed to demonstrate the capabilities of quadrocopter air sampling for analysing the methane isotopic composition in the laboratory. Boundary layer mixing processes and the methane isotopic composition were studied with a quadrocopter system at Polder Zarnekow in Mecklenburg–West Pomerania in the North East of Germany, which has become a strong source of biogenically produced methane after rewetting the drained and degraded peatland. Methane fluxes are measured continuously at the site. They show high emissions from May to September, and a strong diurnal variability with maximum methane fluxes up to $2\,\mu\mathrm{mol}\,\mathrm{m}^{-2}\,\mathrm{s}^{-1}$ for summer 2018. For two case studies on 23 May 2018 and 5 September 2018, vertical profiles of temperature and humidity were recorded up to an altitude of 650 m and 1000 m, respectively, during the morning transition. Air samples were taken at different altitudes and analysed in the laboratory for methane isotopic composition. The values showed a different isotopic signature in the vertical distribution during stable conditions in the morning (-51.5‰ below the temperature inversion at an altitude of 150 m on 23 May 2018 and at an altitude of 50 m on 5 September 2018, -50.1‰ above). After the onset of turbulent mixing, the isotopic signature was the same throughout the vertical column with a mean value of -49.9 ± 0.45‰. During the September study, water samples were analysed as well for methane concentration and isotopic composition in order to provide a link between surface and atmosphere. The water samples reveal high variability on scales of few 10 m for this particular case. The airborne sampling system and consecutive analysis chain were shown to provide reliable and reproducible results for two samples obtained simultaneously. The method presents a powerful tool for constraining the origin of methane by analysing its isotopic signature, and for measuring the vertical distribution of methane isotopic signature, which is based on mixing processes of methane within the atmospheric boundary layer.

1 Introduction

Methane's (CH_4) global warming potential is 32 times higher than carbon dioxide (CO_2) on a century timescale (Etminan et al., 2016), and 72 times higher on a decadal time scale (Solomon et al., 2007) producing a near-future, greater overall impact on the atmospheric radiative balance (Solomon et al., 2007). As a result, CH_4 regulation has a far higher potential for near-term climate change mitigation than CO_2. Moreover, global warming feedbacks and rising anthropogenic emissions will likely increase CH_4 emissions (Wunch et al., 2009). Yet, current knowledge of CH_4 sources remains inadequate. This is in part caused by the complex processes of production, transformation and transport, and in part caused by the lack of sufficiently accurate assessments of the vertical distribution of methane and the temporal and spatial behaviour of highly variable anthropogenic and natural CH_4 surface fluxes (Solomon et al., 2007). Global mean CH_4 concentration increased until the early 1990s, then mostly stabilized for about a decade (Dlugokencky et al., 2003). Since 2007, growth has resumed (Dlugokencky et al., 2013), which is visible in the remote polar areas as well (Nisbet et al., 2016). The stabilization was proposed to have been a consequence of reduction in methane emissions from Siberian gas fields and other sources inside the Soviet Union after its collapse, changes in rice agriculture, and changes in microbial emissions (Dlugokencky et al., 2009). The recent increase has been proposed to be related to enhanced emissions from tropical wetlands associated with the extremely wet season in 2009 in the Amazon region (Dlugokencky et al., 2009; Chen et al., 2010).

For separating natural and anthropogenic emission, the methane isotopic signature $\delta^{13}C\,\permil$ is of particular interest: Biologically produced methane has a typical $\delta^{13}C$ ratio of -70 to -55 ‰ (France et al., 2016; Nisbet et al., 2016), methane from fossil fuels has a typical value of -55 to -25 ‰ (Kirschke et al., 2013), and methane from fires has values of -25 to -13 ‰ (Kirschke et al., 2013; Nisbet et al., 2016). Further, smaller differences in the isotopic signature are observed for different geographic regions. The backgound value of air in the free troposphere currently has a value of around -47.4 ‰ at northern latitudes (Nisbet et al., 2016). The isotopic shift towards depleted (lower, more negative) $\delta^{13}C$ values provides evidence of predominantly biogenic origin (Nisbet et al., 2016).

The origin of methane and the importance of different natural sources is under discussion for various locations worldwide. Known sources in northern latitudes are permafrost areas (Sachs et al., 2010; France et al., 2016; Sasaki et al., 2016; Kohnert et al., 2018), the Arctic ocean (Yu et al., 2015; Mau et al., 2017) and wetlands (Bellisario et al., 1999). Each source region has a unique isotopic signature, and mixing of different air masses results in a linear combination of the corresponding $\delta^{13}C$ signature (France et al., 2016). In the Arctic, inter-annual shifts in the sea ice drift patterns generate an inter-annually patchy methane excess in polar surface water and methane efflux (Damm et al., 2018). The origin of this enhanced methane concentration and the exchange processes between ocean, atmosphere and sea ice are subject to current investigation (Mau et al., 2017; Uhlig and Loose, 2017; Platt et al., 2018). The exchange of gas between air and sea strongly depends on the water stratification (Andersson et al., 2017). Further, isotopic fractionation towards depletion of $\delta^{13}C$ in the range of few to several ‰ is observed at the water-air interface for diffusion processes (Happell et al., 1995)

In this context, unmanned aerial systems (UAS) fill an observational gap for methane mixing processes. They are able to sample small scales with a typical horizontal distance of 1 km, if they are required to be operated in the line of sight, and they reach

the top of the atmospheric boundary layer, with a maximum altitude of typically around 1 km. First applications of measuring the methane concentration with UAS have been demonstrated: The air sampling inlet integrated into multirotor systems is either directly connected to the ground-based methane analyser via a sampling line (Brosy et al., 2017), or the air is stored in a tubing, which is analysed after the flight with a cavity ring down spectrometer (Andersen et al., 2018). The limiting element for

5 both techniques is the length and weight of the sampling line or tube, and sampling altitudes up to 50 m have been published (Brosy et al., 2017; Wolf et al., 2017; Andersen et al., 2018). An air sampling concept based on filling evacuated stainless steel containers by remotely opening a valve and subsequent chemical analyses of trace gases and first applications on multicopter systems have been shown (Chang et al., 2016, 2018). In-situ methane analysers small enough to be integrated on a UAS have been presented (Gurlit et al., 2005; Miftah El Khair et al., 2017; Graf et al., 2018), and first scientific articles showing field

10 measurements of in-situ multicopter borne methane concentrations up to an altitude of 600 m have been published (Golston et al., 2017). The method of air sampling and methane isotopic analyses has been applied to (manned) airborne measurements with high payload capacity in the lower troposphere, e.g. above Siberian peatlands to distinguish emissions from fossil and biogenic emissions (Umezawa et al., 2012), up to balloon borne observations to study sink mechanisms of methane in the stratosphere (Sugawara et al., 1997).

15 To contribute to constraining the source and vertical mixing processes of methane at different locations, a quadrocopter borne sampling system has been developed. The aim is in-situ air sampling for obtaining the vertical distribution of the methane isotopic ratio in the lower troposphere (up to 1 km) for subsequent laboratory analyses. The goal of the study is two-fold: On the one hand to show the reliability of the measurement chain from the airborne sampling to the laboratory methane isotopic analyses, on the other hand to provide new insights into small-scale methane dynamics at the study site. In order to test the

20 system's capabilities of providing reliable vertical profiles of the isotopic signature, measurements were performed at a rewetted peatland site, Polder Zarnekow (Zerbe et al., 2013), which is known as a source of biologically produced methane. Under stable stratification, it is expected that the methane isotopic ratio is depleted for this source, whereas above the temperature inversion, an isotopic ratio typical of mixed air masses is expected. During the morning transition, when the stable stratification is gradually replaced by a convectively mixed atmospheric boundary layer, the isotopic signature should adjust to a consistent

25 value throughout the profile within the uncertainties of laboratory air sample isotopic analyses.

2 Methods

In the following, the quadrocopter ALICE (Airborne Tool for Methane Isotopic Composition and Polar Meteorological Experiments) as the carrier system, the payload consisting of the air sampling subsystem and the meteorological sensors and data acquisition are described. Further, the laboratory air analysis procedures, and the measurement site for system tests are in-

30 troduced. For evaluating the whole measurement chain, a local source of methane of particular isotopic composition, and atmospheric conditions that first inhibit and then enforce vertical mixing processes (morning transition) were required. These conditions were met at Polder Zarnekow on 23 May 2018. For confirming the results, the same measurement strategy was applied to the same site on 5 September 2018.

2.1 Quadrocopter ALICE and instrumentation

The quadrocopter ALICE (Fig. 1) was designed to carry meteorological sensors and 12 glass bottles for air sampling. It has dimensions of 1.56 m x 1.56 m x 0.38 m without scientific payload. The arms are quickly removable (rotating lock) for convenient storage and transport. It was developed for a maximum take-off weight of 25 kg. For the operations presented here, the

5 total weight was 19 kg, with 4 kg the quadrocopter system itself, 7.2 kg of LiPo batteries with a total capacity of 21 Ah and a nominal voltage of 44.4 V, and 7.8 kg payload including a safety parachute of 12 m^2. The payload is placed in the center of the system on a platform with dimensions of 370 mm x 210 mm. The temperature and humidity sensors are located in a housing to shield against radiation and protect against impact of dust at the edge of the platform. An electronics box contains the central data acquisition.

10 The quadrocopter is constructed with a thrust-to-weight ratio of 2:1. The system was designed for wind speeds up to 35 km h^{-1} during take-off and landing, and up to 70 km h^{-1} during free flight. At a wind speed of 60 km h^{-1}, a climb rate of the current system of 8 m s^{-1} was still possible. ALICE is electrically powered with four motors U11 KV120 of T-Motor, China.

As the system was intended for operations in the polar regions, the design point of the system is -30 °C. All parts have been tested extensively in a climate chamber down to -30 °C, taking into account vibrations of the carrier, which were simulated

15 with a shaker after in-flight measurements. The batteries are insulated passively, and the temperatures of the batteries and the internal avionics are monitored.

Air temperature is recorded with various temperature sensors of different behaviour. Fast fine wire temperature sensors, manufactured at the Institute of Flight Guidance (Bärfuss et al., 2018), have the advantage of high temporal resolution up to 100 Hz. Further, standard long-term stable sensors were used (Pt1000 "Humicap" HMP110, Vaisala, Finland, digital sensor TSYS01,

20 Measurement Specialities, US). Relative humidity is measured with two different sensors, the Humicap HMP110 (Vaisala, Finland), and the Rapid P14 (Innovative Sensor Technology, Switzerland). Absolute pressure is recorded with AMSYS 5812-0150-B sensors, AMSYS, Germany. Two pyranometers ML-01 of EKO Instruments, Japan, with nadir and zenith viewing geometry are integrated, which allow to estimate cloudiness and surface properties at a sampling rate of 100 Hz. Further, a surface temperature sensor Melexis MLX90614, Belgium, is mounted into the airframe and fixed at the bottom of the UAS. A

25 Global Navigation Satellite System (GNSS) receiver and an inertial measurement unit (IMU) iμVRU of iMAR, Germany, are integrated. Data is recorded at a sampling frequency of 100 Hz.

The air sampling system consists of 12 glass flasks (sample containers) evacuated before take-off. They are equipped with two manual valves. Directly before the mission, each glass flask is linked with a vacuum pump RE5 of Vacuubrand, Germany. One valve is left open, and an electromagnetic valve is connected, which is normally closed. Then the flask is evacuated, and the

30 pressure is controlled by a pressure sensor integrated in the electromagnetic valve. The flasks are opened during the flight with magnet valves, that are triggered either manually by remote control or automatically at altitudes predefined by the operator. After triggering, ambient pressure is reached within less than 2 s. The pressure sensors integrated in the valves are used to monitor air tightness. The most critical point were the manual plastic valves deployed routinely for the glass flasks in open position. They had to be treated individually and controlled to make sure that no leakage occurred during the mission. For

quality control and redundance, two glass flasks were filled simultaneously, resulting in six possible sampling altitudes during one flight. The whole quadrocopter system with technical details and instrumentation is shown in Fig. 2.

The data are displayed at the ground station. Depending on the atmospheric structure, the operator decides on the altitude of taking samples during the descent, e.g. above/below the temperature inversion, or within altitudes of enhanced humidity, as

5 required for the scientific question. The evacuated flasks are opened by electromagnetical valves via telemetry command at specific altitudes or by remote control. The whole mission can be flown automatically by a PixHawk autopilot. It is supervised by a safety pilot and a scientific operator who is controlling the system and performance as well as the measurements. Two small cameras, one pointing downwards (GoPro HERO5 Black, 12 Megapixel), one looking to the side (GoPro HERO Session Actionkamera, 8 Megapixel), were integrated. The captured video of the downward pointing camera was transmitted to the

10 operator with 720p resolution and 60 Hz. There are different telemetry connections: A 2.4 GHz link is used for the remote control. A 868 MHz connection serves to send commands to the autopilot, and a 868 MHz link is used for activating the safety parachute trigger. Further, a 5 GHz video link is established. Scientific data are transmitted via an additional 868 MHz connection.

2.2 Laboratory isotopic analyses

The $\delta^{13}C$ methane signature in air samples was analyzed using a Delta plus XP mass spectrometer combined with a combustion oven, a gas pressure interface and a pre-concentration device (PreCon) (ThermoFinnigan, Bremen, Germany). All valves and traps are automatically operated by the mass spectrometer software. Following the quadrocopter mission, the sample containers (SC) were transported to the laboratory at the Alfred Wegener Institute in Bremerhaven, Germany. Each SC was installed onto

20 the PreCon and the connections were flushed with helium before the SC was opened. The air sample was first carried by helium carrier gas through a chemical trap and then trapped in a cool box filled with liquid nitrogen (-196°C) to remove CO_2, CO and H_2O. Afterwards the CO_2 free air was carried by helium carrier gas to the combustion oven (1000°C) for methane conversion into CO_2 which then was purged into a second cool box filled with liquid nitrogen and trapped therein. When the combustion is finished, the gas stream is purged and trapped in a third cool box filled with liquid nitrogen to pre-concentrate the sample,

25 and carried by helium carrier gas into the isotope ratio mass spectrometer. Methane stable carbon isotope data are given in δ notation (in ‰) relative to the Pee Dee Belemnite (PDB) standard:

$$\delta^{13}C‰ = \left(\frac{\frac{^{13}C}{^{12}C}sample}{\frac{^{13}C}{^{12}C}reference} - 1\right) \cdot 1000 \qquad (1)$$

Precision, determined by repeated analysis of Bremerhaven air is about 0.5‰. Further applications of the system have been described in Mau et al. (2013); Damm et al. (2015); Verdugo et al. (2016); Fenwick et al. (2017).

2.3 Study site, water sampling, and flight strategy

30

The shallow Polder Zarnekow with a water depth of less than 1 m belongs to a large area of rewetted peatlands in the Peene River valley in North-Eastern Germany (53°52.5' N 12°53.3' E, less than 0.5 m a.s.l). It formed after the dikes were opened in

2004/05 in order to restore the peatlands, taking up CO_2 to reduce the sources of greenhouse gases. The site is a Fluxnet site (DE-Zrk) and is part of the Northeast German Lowland observatory of the Terrestrial Environmental Observatories Network TERENO (Heinrich et al., 2018).

It is equipped with state of the art eddy covariance (EC) instrumentation recording the wind vector, temperature and the
5   concentration of water vapour, CH_4 and CO_2 at a frequency of 20 Hz. The measurement height above the water surface is around 2.6 m, depending on the water level. Water vapour and CO_2 are measured with a LI-7200 sensor of LI-COR, US. Methane is measured with a LI-COR sensor LI-7700. Further, a Los Gatos Fast Greenhouse Gas Analyser (FGGA, US) records the concentration of the three greenhouse gases at a frequency of 20 Hz. Four automatic measurement chambers are installed along a transect between the EC system and the shore of the lake for spatially resolved CO_2 and CH_4 flux investigations
10 (Hoffmann et al., 2017).

The restoration of the peatland area towards a net sink of greenhouse gases, and in particular CH_4, is a process of several years to decades, which strongly depends on vegetation and the water level (Couwenberg et al., 2011; Zak et al., 2015). The shallow eutrophic lake in particular acts as a strong source of CH_4 (Franz et al., 2016). Maximum methane emissions are typically observed in summer (Franz et al., 2016). In the diurnal cycle, the maximum CH_4 emissions were recorded during night (Franz
15 et al., 2016). This is in agreement with stronger convective mixing of the lake induced thermally from May to October (Franz et al., 2016), which leads to diffusive CH_4 emissions (Hoffmann et al., 2017).

The time series of methane fluxes of the 3-year period 2016 to 2018 (Fig. 3) reveal a high variability over the entire period and within time periods of few days, with noticeable fluxes during the growing season between May and September.

For identifying the reason for small-scale inhomogeneities of the atmospheric methane isotopic ratio, the methane source
20 located within the surface water was sampled at different locations on 5 September 2018. Six water samples were taken with Kemmerer glass bottles of 50 ml at the locations Z-1 to Z-6 indicated in Fig. 4. After filling and locking with screw cap, the water samples were stored and transported light-tight in a cool box. They were analysed in the laboratory for methane concentration and isotopic composition at the Alfred Wegener Institute in Bremerhaven on 6 and 7 September 2018, thus directly after the sampling.

25 The aerial measurement strategy consists of an automatic climb flight up to 1 km altitude and down again with real-time data transmission of selected parameters at 1 Hz. For the missions presented here, a permission from the nature protection agency and coordination with the German Civil Aviation Agency (DFS, Deutsche Flugsicherung) were required.

On 23 May 2018, three consecutive measurement flights of around 10-11 min duration were performed over a time period of 3 h in the morning, with take-off times 06:04, 07:30, and 08:29 and UTC, corresponding to a local time between 08:04 and
30 10:29. Sunrise was at 04:55 local time.

Each flight consisted of manual take-off and climb up to around 50 m altitude, then handing over the mission to the autopilot. The flight pattern followed 3 waypoints at 50 m altitude leading to a position directly above the open water fraction of the polder. There, a vertical ascent with a mean vertical speed of $5 \, \mathrm{m \, s^{-1}}$ up to a height of 650 m agl and subsequent descent with a vertical speed of $-2 \, \mathrm{m \, s^{-1}}$ took place. For this feasibility study, air samples were taken during descent at the approximate
35 altitudes of 600 m, 400 m, 300 m, 200 m, 100 m and 10 m. Then the quadrocopter flew to a waypoint close to the landing point

and was landed manually. The air samples were analysed in the laboratory for methane isotopic composition at the Alfred Wegener Institute in Bremerhaven on 11, 12 and 13 June 2018, thus 3 weeks after the sampling.

On 5 September 2018, five consecutive measurement flights of around 12-13 min duration were performed over a time period of 5 h in the morning, with take-off times 06:04, 07:15, 09:12, 10:05 and 10:57 UTC, corresponding to a local time between

5   08:04 and 12:57. Sunrise was at 06:23 local time. The same flight strategy as described above was applied. However, the ascents reached an altitude of 1000 m. The vertical ascents were done with a mean vertical speed of 6.5 m s^{-1} and the descents with a vertical speed of -2 m s^{-1}.

3   Results

3.1   Synoptic conditions and meteorological observations

10   On 23 May 2018, the synoptic situation was characterized by a pronounced high-pressure system above Scandinavia and the Baltic Sea, leading to conditions of low wind speed below 5 m s^{-1}, north-easterly wind directions and a cloudless sky, as evidenced from the smooth behaviour of global radiation (Fig. 5).

On 5 September 2018, the synoptic situation was determined by two strong high pressure systems located above the Atlantic Ocean and above Northern Russia, and a low-pressure system above Southern Europe. This resulted in low wind speed below

15   4 m s^{-1} of north-easterly direction at the observation site, similar to the conditions on 23 May 2018. In the morning, until 05:30 UTC, around 30 min before the first flight, fog was observed, which was denser towards the East. Starting around 09:00, before flight 3, shallow convective cumulus clouds were present. This is also evident in the high variability of the global radiation (Fig. 6).

On 23 May 2018, the near-surface temperature increased from around 13-14° C at 6 UTC to around 17° C at 08:30 UTC (Fig.

20   7). The profiles of potential temperature show a strongly stable stratification in the morning, with an increase of potential temperature of around 2 ° C (06:04 UTC) from the surface to 250 m. The top of the nocturnal temperature inversion was located at around 150 to 250 m altitude. At this altitude range, the water vapour mixing ratio decreased as well from around 7 g kg^{-1} in the boundary layer close to the surface to around 5 g kg^{-1} above. After 07:30 UTC, the atmosphere was less stably stratified. The water vapour mixing ratio was enhanced in the lowermost 150 m at 06:04 UTC. Above and later, the water vapour mixing

25   ratio was almost constant with height.

On 5 September 2018 during the first flight, the profiles show a mixed-layer up to 50 m altitude and a stable stratification above (Fig. 8). The water vapour mixing ratio was lower in the mixed layer (11 g kg^{-1}) and increased above up to 14 g kg^{-1}. For the following four flights, the near surface temperature increased, and the potential temperature increased only slightly with altitude. The water vapour mixing ratio decreased with time throughout the whole profile.

30

3.2 Observations of methane emissions and isotopic signature

For both observation days, the methane concentration recorded at the eddy covariance tower at 2.6 m altitude above the surface shows a high variability during the night and the morning, and a relatively constant concentration during the day. During the time period of the first flight on 23 May 2018, the methane concentration was still slightly enhanced compared to the

5   background value during the day (Fig. 9). The first flight on 5 September 2018 took place during the high fluctuations of the CH_4 concentration (Fig. 10).

The isotopic signature of the air samples was different during the first flight of each day at the altitudes located within the stable stratification. On 23 May 2018, the isotopic ratio was depleted at 10 m and 100 m altitude with a value of -51.5‰ (see Fig. 11). Above, the mean isotopic ratio was -50.1‰, almost the same as during the next flights throughout the profile, with an average

10   value of -49.9‰. On 5 September 2018, the same systematic behaviour was observed: During the first flight, the isotopic ratio was depleted at an altitude of 10 m, in agreement with a temperature inversion above an altitude of 50 m. Above, the isotopic value of -49.9‰ was the same as during all other flights throughout the profile (Fig. 12).

Aerial pictures obtained during the measurement flights for the two case studies show the difference in water level: On 23 May 2018, the lake was filled with water (Fig. 13). On 5 September 2018, almost the whole lake had fallen dry, with only few wet

15   areas remaining, and the sediment still saturated with water (Fig. 4). The depth was in the range of few cm.

The water samples taken on 5 September 2018 within a radius of 100 m revealed highly different CH_4 concentrations (see Table 1). The highest CH_4 concentration of around 4770 ppm was measured from the water sample Z-4 in one of the small remaining water areas with a depth less than 5 cm within the former polder. Directly next to this, the water sample Z-3 taken at a depth of 5-10 cm had a methane concentration of 2310 ppm (see Figs. 4 for exact locations). The water sample Z-4 contained

20   more suspended sediment load than sample Z-3. The sample sites are located within small remaining water areas, which are not connected.

4   Discussion

4.1   Plausibility of the observed isotopic signature

The methane flux data indicate that the observation site was a source of methane during both measurement days, but had

25   much higher emissions on 23 May 2018 (Fig. 14). During the first flights in the early morning, under stable stratifications, an enhanced methane concentration in the ABL can be expected, as observed by Andersen et al. (2018) above wetlands. This is the case on both measurement days with the UAS. An enhanced methane concentration and high variability was observed until around 06:30 UTC on 23 May 2018 (Fig. 9), and even higher concentrations and stronger fluctuations were observed until 6:45 UTC on 5 September 2018 (Fig. 10). Under stable atmospheric conditions during the night and in the early morning hours,

30   the near-surface methane concentration is enhanced, as no vertical mixing is possible, e.g. Emeis (2008); Brosy et al. (2017). With a local methane source, the near-surface methane concentration above agricultural land therefore increases during stable atmospheric conditions (Wolf et al., 2017), as this prevents dilusion with the free troposphere. However, a high local horizontal

inhomogeneity in methane concentrations resulting from mixed-use areas have been reported, an effect which is visible in the lowermost 10 m above the surface, but smeared out above due to an increase in horizontal wind speed (Wolf et al., 2017). A high variability of methane sources is in agreement with the highly variable methane water concentrations measured within a radius of 100 m on 5 September 2018.

5 The isotopic difference obtained for air samples near ground and above the temperature inversion during stable stratification is around 1.5‰, thus significantly higher than the uncertainties (flight 1 for each measurement day). This shows that the observed systematic differences are real measurement features, not measurement uncertainty.

Assuming that the parts of the surface with high methane concentrations, like sample Z-3, Z-4 and Z-6, act as a methane source, with an isotopic ratio of around -48 to -49‰ (water sample Z-4 and Z-6), an isotopic fractionation of around 3‰ would occur

10 across the water-air boundary. This is in the order of magnitude of carbon isotope depletion observed for emitted relative to floodwater CH_4, ranging from 1.8 to 3.4‰ (Happell et al., 1995), thus can be considered realistic.

4.2 Interpretation of isotopic signature from measurement point of view

Generally, the isotopic ratios of the two air samples taken simultaneously but with a constant horizontal distance of 13 cm at the lowest altitude of 10 m agree to within 0.2‰ (Fig. 11 and Fig. 12). However, during flight 1 on 23 May 2018, parallel to the

15 high variability of the methane concentration, and flight 5 on 5 September 2018, the isotopic signature of the two air samples taken simultaneously at 10 m altitude reveal a significant isotopic difference of 0.75‰. As the repeatability of the isotopic ratio of samples taken within identical air masses is 0.5‰, this difference is larger than the uncertainty, and therefore the systematic differences are treated as features. There are several striking features in the profiles of isotopic signatures:

- The isotopy ratio has more negative values in the morning before vertical mixing starts, as long as a temperature inversion

20   is present (first flight on 23 May 2018 below 150 m, and first flight on 5 September 2018 below 70 m). This is in agreement with methane from biologic processes emitted from the surface that are not vertically mixed.

- The difference in isotopic ratio between the two simultaneous samples is systematically smaller at 10 m altitude compared to the higher altitudes on 5 September 2018, except the last profile.

- The differences in isotopic ratio at 100 m altitude increase during the course of the day on 5 September 2018.

25 The hypothesis is that the air samples obtained at 10 m altitude are influenced by air masses representative of a smaller, thus more homogeneous area. At an altitude of 100 m, air masses are influenced by a similarly small area, as long as stable stratification is present. With increasing turbulent mixing, a different footprint influences the air masses, and small-scale inhomogeneities can impact measurements only 13 cm apart. Episodic CH_4 ourbursts on short time scales of few min have been observed by Schaller et al. (2018). The high spatial and temporal variability of methane emissions reported here confirm their

30 observations.

5 Conclusions

The measurements serve both as a proof of concept for the system and show the vertical mixing of methane in the ABL by means of its isotopic signature. With ALICE air samples and subsequent laboratory analyses, it is possible to determine differences in the methane isotopic signature in agreement with atmospheric stability. For the future, a combination of in-situ

5 high resolution methane concentration measurements and air sampling for isotopic analyses is required for substantial progress in understanding vertical exchange and trace back methane concentrations to specific sources and sinks in the atmospheric boundary layer.

The differences in isotopic values of water and air, the differences in isotopic values between both flight days and the development during each day emphasize the highly complex and inhomogeneous nature of methane processes on horizontal

10 scales below 1 km in sediments, at the sediment-water and the water-atmosphere border. Therefore, the representativeness of individual methane flux measurements have to be treated with care, and footprint analyses are required to extrapolate the measurements on a larger area. Vertical layering of air masses with different methane properties strongly depends on atmospheric stability, both concerning concentration as well as the isotopic ratio. A holistic approach is needed to approach methane processes from sediments to the atmospheric boundary layer, including dedicated measurements of the isotopic fractionation.

15 *Data availability.* The data of the flight is available upon request from the authors of TU Braunschweig. Biomet and flux data will be uploaded to the European Fluxes Database Cluster (http://www.europe-fluxdata.eu/) and the TERENO Data Portal (http://teodoor.icg.kfa-juelich.de/ddp/) after final processing and quality control.

Author contributions. AL wrote the paper, FP developed the quadrocopter payload, TK developed the quadrocopter, FP, TK, TR, AL and MA conducted the measurement campaigns, FP and ED performed the laboratory methane isotope analyses, CW and TS performed the

20 methane flux measurements, LL performed the quality check of the copter measurements. All authors contributed to and commented on the manuscript.

Competing interests. The authors declare that they have no conflict of interest.

Acknowledgements. The development of the quadrocopter was funded by the German Research Foundation (DFG) in the framework of the priority programme "Antarctic Research with comparative investigations in Arctic ice areas" under grant LA 2907/8-1, DA 1569/1-2. The

25 authors would like to thank Barbara Altstädter for critically reading the manuscript.

References

Andersen, A., Scheeren, B., Peters, W., and Chen, H.: A UAV-based active AirCore system for measurements of greenhouse gases, Atmos. Meas. Tech., 11, 2683-2699, 2018.

Andersson, A., Falck, E., Sjöblom, A., Kljun, N., Sahlée, E., Omar, A.M., and Rutgersson, A.: Air-sea gas transfer in high Arctic fjords, Geophys. Res. Lett., 10.1002/2016GL072373, 8 pp., 2017.

Bärfuss, K., Pätzold, F., Altstädter, B., Kathe, E., Nowak, S., Bretschneider, L., Bestmann, U., and Lampert, A.: New Setup of the UAS ALADINA for Measuring Boundary Layer Properties, Atmospheric Particles and Solar Radiation, Atmosphere, 9, 28, doi:10.3390/atmos9010028, 21 pp., 2018.

Bellisario, L.M., Bubier, J.L., and Moore, T.R.: Controls on CH_4 emissions from a northern peatland, Global Biogeochemical Cycles, 13, 1, 81-91, 1999.

Brosy, C., Krampf, K., Zeeman, M., Wolf, B., Junkermann, W., Schäfer, K., Emeis, S., and Kunstmann, H.: Simultaneous multicopter-based air sampling and sensing of meteorological variables, Atmos. Meas. Tech., 10, 2773-2784, 2017.

Chang, C.-C., Wang, J.-L., Chang, C.-Y., Liang, M.-C., and Lin, M.-R.: Development of a multicopter-carried whole air sampling apparatus and its applications in environmental studies, Chemosphere, 144, 484–492, 2016.

Chang, C.-C., Chang, C.-Y., Wang, J-L., Lin, M.-R., Ou-Yang, C.-F., Pan, H.-H., and Chen, ,Y.-C.: A study of atmospheric mixing of trace gases by aerial sampling with a multi-rotor drone, Atmospheric Environment, 184, 254-261, 2018.

Chen, J., Wilson, C., and Tapley, B.: The 2009 exceptional Amazon flood and interannual terrestrial water storage change observed by GRACE. Water Resour Res. 46: W12526, doi:10.1029/2010WR009383, 2010.

Couwenberg, J., Thiele, A., Tanneberger, F., Augustin, J., Bärisch, S., Dubovik, D., Liashchynskaya, N., Michaelis, D., Minke, M., Skuratovich, A., and Joosten, H.: Assessing greenhouse gas emissions from peatlands using vegetation as a proxy, Hydrobiologia, 674, 67-89, 2011.

Damm, E., Rudels ,B., Schauer, U., Mau, S. and Dieckmann, G.: Methane excess in Arctic surface water- triggered by sea ice formation and melting. Scientific Reports 5:16179 | doi: 10.1038/srep16179, 2015.

Damm, E., Bauch, D., Krumpen, T., Rabe, B., Korhonen, M., Vinogradova, E.L. and Uhlig, C. : The Transpolar Drift conveys methane from the Siberian Shelf to the central Arctic Ocean, Scientific Reports, 8, doi:10.1038/s41598-018-22801-z, 10 pp., 2018.

Dlugokencky, E., Houweling, S., Bruhwiler, L., Masarie, K., Lang, P., Miller, J.,,and Tans, P.: Atmospheric methane levels off: Temporary pause or a new steady-state? Geophys Res Lett., 30, 1992, doi:10.1029/2003GL018126, 2003.

Dlugokencky, E., Bruhwiler, L., White, J., Emmons, L., Novelli, P., Montzka, S., Masarie, K., Lang, P., Crotwell, A., Miller, J., and Gatti, L.: Observational constraints on recent increases in the atmospheric CH4 burden. Geophys Res Lett. 36: L18803, 2009.

Dlugokencky, E., Crotwell, A., Masarie, K., White, J., Lang, P., and Crotwell M.: NOAA Measurements of Long-lived Greenhouse Gases, Asia-Pacific GAW Greenhouse Gases, 6: 6-9, 2013.

Emeis, S.: Examples for the determination of turbulent (sub-synoptic) fluxes with inverse methods, Meteorol. Z., 17, 1, 003-011, 2008.

Etminan, M., Myhre, G., Highwood, E.J., and Shine, K.P.: Radiative forcing of carbon dioxide, methane, and nitrous oxide: A significant revision of the methane radiative forcing, Geophys. Res. Lett., 10.1002/2016GL071930, 2016.

Fenwick, L., Capelle, D., Damm E., Zimmermann, S., William J. Williams, W.J., Vagle, S. and Tortell, P.D.: Methane and nitrous oxide distributions across the North American Arctic Ocean during summer, 2015. J. Geophys. Res. Oceans, 122, doi:10.1002/2016JC012493, 2017

France, J.L., Cain, M., Fisher, R.E., Lowry, D., Allen, G., O'Shea, D.J., Illingworth, S., Pyle, J., Warwick, N., Jones, B.T., Gallagher, M.W., Bower, K., Le Breton, M., Percival, C. Muller, J., Welpott, A., Bauguitte, S., George, C., Hayman, G.D., Manning, A.J., Lund Myhre, C., Lanoiselle, M., and Nisbet, E.G.: Measurements of δ^{13}C in CH_4 and using particle dispersion modelingg to characterize sources of Arctic methane within an air mass, J. Geophys. Res. Atmos., 121, 144,257-14,270, 2016.

5   Franz, D., Koebsch, F., Larmanou, E., Augustin, J., and Sachs, T.: High net CO_2 and CH_4 release at a eutrophic shallow lake on a formerly drained fen, Biogeosciences, 13, 3051-3070, 2016.

Graf, M., Emmenegger, L., and Tuzson, B.: Compact, circular, and optically stable multipass cell for mobile laser absorption spectroscopy, Opt. Lett. 43, 2434-2437, 2018.

Golston, L.M., ,Tao, L., Brosy, C., Schäfer, K., Wolf, B., McSpiritt, J., Buchholz, B., Caulton, D.R., Pan, D., Zondlo, A., Yoel, D., Kunstmann,
10   ,H., and McGregor, M.: Lightweight mid-infrared methane sensor for unmanned aerial systems, Appl Phys B Lasers Opt 123,1–9. doi: 10.1007/s00340-017-6735-6, 2017.

Gurlit, W., Zimmermann, R., Giesemann, C., Fernholz, T., Ebert, V., Wolfrum, J., Platt, U., and Burrows, J.P.: Lightweight diode laser spectrometer CHILD (Compact High-altitude In-situ Laser Diode) for balloonborne measurements of water vapor and methane, Appl. Opt., 44, 1, 91-102, 2005.

15   Happell, J.D., Chanton, J.P., and Showers, W.J.: Methane transfer across the water-air interface in stagnant wooded swamps of Florida: Evaluation of mass-transfer coefficients and isotopic fractionation, Limnol. Oceanogr., 40(2), 290-298, 1995.

Heinrich, I., Balanzategui, D., Bens, O., Blasch, G., Blume, T., Böttcher, F., Borg, E., Brademann, B., Brauer, A., Conrad, C., Dietze, E., Dr"ager, N., Fiener, P., Gerke, H. H., G/"untner, A., Heine, I., Helle, G., Herbrich, M., Harfenmeister, K., Heußner, K., Hohmann, C., Itzerott, S., Jurasinski, G., Kaiser, K., Kappler, C., Koebsch, F., Liebner, S., Lischeid, G., Merz, B., Missling, K. D., Morgner, M.,
20   Pinkerneil, S., Plessen, B., Raab, T., Ruhtz, T., Sachs, T., Sommer, M., Spengler, D., Stender, V., Stüve, P., and Wilken, F.: Interdisciplinary Geo-ecological Research across Time Scales in the Northeast German Lowland Observatory (TERENO-NE), Vadose Zone Journal, 17, 1, 1-25, 2018.

Hoffmann, M., Schulz-Hanke, M., Garcia Alba, J., Jurisch, N., Hagemann, U., Sachs, T., Sommer, M., and Augustin, J.: A simple calculation algorithm to separate high-resolution CH_4 flux measurements into ebullition- and diffusion-derived components, Atmos. Meas. Tech., 10,
25   109-118, 2017.

Kirschke, S., Bousquet, P., Ciais, P., Saunois, M., Canadell, J.G., Dlugokencky, E.J., Bergamaschi, P., Bergmann, D., Blake, D.R., Bruhwiler, L., Cameron-Smith, P., Castaldi, S., Chevallier, F., Feng, L., Fraser, A., Heimann, M., Hodson, E.L., Houweling, S., Josse, B., Fraser, P.J., Krummel, P.B., Lamarque, J.-F., Langenfelds, R.L., Le Quere, C.,, Naik, V., O'Doherty, S., Palmer, P.I., Pison, I., Plummer, D., Poulter, B., Prinn, R.G., Rigby, M., Ringeval, B., Santini, M., Schmidt, M., Shindell, D.T., Simpson, I.J., Spahni, R., Steele, L.P., Strode, S.A.,
30   Sudo, K., Szopa, S., van der Werf, G.R., Voulgarakis, A., van Weele, M., Weiss, R.F., Williams, J.E., and Zeng, G.: Three decades of global methane sources and sinks, Nature Geoscience, 6, 813-823, 2013.

Kohnert, K., Juhls, B., Muster, S., Antonova, S., Serafimovich, A., Metzger, S., Hartmann, J., and Sachs, T.: Toward understanding the contribution of waterbodies to the methane emissions of a permafrost landscape on a regional scale - A case study from the Mackenzie Delta, Canada, Global Change Biology, 24, 9, 3976-3989, 2018.

35   Mau, S., Blees, J., Helmke, E., Niemann, H., and Damm, E. 2013: Vertical distribution of methane oxidation and methanotrophic response to elevated methane concentrations in stratified waters of the Arctic fjord Storfjorden (Svalbard, Norway). Biogeosciences, 10, 6267–6278, doi:10.5194/bg-10-6267-2013, 2013.

Mau, S., Römer, M., Torres, M.E., Bussmann, I., Pape, T., Damm, E., Geprägs, P., Wintersteller, P., Hsu, C.-W., Loher, M., and Bohrmann, G.: Widespread methane seepage along the continental margin off Svalbard - from Bjørnøya to Kongsfjorden, Scientific Reports, 7:42997, doi:10.1038/srep42997, 2017.

Miftah El Khair, Z., Joly, L., Cousin, J., Decarpenterie, T., Dumelié, N., Maamary, R., Chauvin, N., and Durry, G.: In situ measurements of
5   methane in the troposphere and the stratosphere by the Ultra Light SpEctrometer Amulse, Appl. Phys. B, 123, 281, doi:10.1007/s00340-017-6850-4, 11 pp., 2017.

Nisbet, E.G., Dlugokencky, E.J., Manning, M.R., Lowry, D., Fisher, R.E., France, J.L., Michel, S.E., Miller, J.B., White, J.W.C., Vaughn, B., Bousquet, P., Pyle, J.A., Warwick, N.J., Cain, M., Browwnlow, R., Zazzeri, G., Lanoiselle, M., Manning, A.C., Gloor, E., Worthy, D.E.J., Brunke, E.-G., Labuschagne, C., Wolff, E.W., and Ganesan, A.L.: Rising atmospheric methane: 2007-2014 growth and isotopic
10   shift, Global Biogeochem. Cycles, 30, 1356-1370, 2016.

Platt, S.M., Eckhardt, S., Ferré, B., Fisher, R.E., Hermansen, O., Jansson, P., Lowry, D., Nisbet, E.G., Pisso, I., Schmidbauer, N., Silyakova, A., Stohl, A., Svendby, T.M., Vadakkepuliyambatta, S., Mienert, J., and Myhre, C.L.: Methane at Svalbard and over the European Arctic Ocean, Atmos. Chem. Phys., 18, 17207–17224, 2018.

Sachs, T., Giebels, M., Boike, J., and Kutzbach, L.: Environmental controls of CH4 emission from polygonal tundra on the micro-site scale,
15   Lena River Delta, Siberia, Global Change Biology, 16, 11, 3096-3110, 2010.

Sasaki, M., Kim, Y.-W., Uchida, M., Utsumi, M.: Diffusive summer methane flux from lakes to the atmosphere in the Alaskan arctic zone, Polar Science, 10, 303-311, 2016.

Schaller, C., Kittler, F., Foken, F., and Gödecke, M.: Characterisation of short-term extreme methane fluxes related to non-turbulent mixing above an Arctic permafrost ecosystem, Atmos. Chem. Phys. Discuss., https://doi.org/10.5194/acp-2018-277, 2018.

20 Shindell, D.T., Faluvegi, G., Bell, N., and Schmidt, G.A.: An emissions-based view of climate forcing by methane and tropospheric ozone, Geophysical Research Letters 32, L04803, 2005.

Shindell, D.T., Faluvegi, G., Koch, D.M., Schmidt, G.A., Unger, N., and Bauer, S.E.: Improved attribution of climate forcing to emissions, Science, 326, 716-718, 2009.

Solomon, S., Qin, D., Manning, M. Chen, Z., Marquis, M., Averyt, K.B., Tignor, M., and, Miller, H.L. (eds.): Contribution of Working Group
25   I to the Fourth Assessment Report of the Intergovernmental Panel on Climate Change, Cambridge University Press, Cambridge, United Kingdom and New York, NY, USA, 2007.

Sugawara, S., Nakazawa, T., Shirakawa, Y., Kawamura, K., and Aoki, S.: Vertical profile of the carbon isotopic ratio of stratospehric methane over Japan, Geophys. Res. Lett., 24, 23, 2989-2992, 1997.

Uhlig, C., and Loose, B.: Using stable isotopes and gas concentrations for independent constraints on microbial methane oxidation at Arctic
30   Ocean temperatures, Limnol. Oceanogr.: Methods, 15, 737-751, 2017.

Umezawa, T., Machida, T., Aoki, S., and Nakazawa, T.: Contributions of natural and anthropogenic sources to atmospheric methane variations over western Siberia estimated from its carbon and hydrogen isotopes, Glocal Biogeochemical Cycles, 26, GB4009, doi:10.1029/2011GB004232, 15 pp., 2012

Verdugo, J., Damm, E., Snoeijsc, P. Diez, B. and Farias, L.: Climate relevant trace gases (N2O and CH4) in the Eurasian Basin (Arctic
35   Ocean). Deep Sea Research I, 117, 84-94, 2016.

Wolf, B., Chwala, C., Fersch, B., Garvelmann, J., Junkermann, W., Zeeman, M.J., Angerer, A., Adler, B., Beck, C., Brosy, C., Brugger, P., Emeis, S., Dannenmann, M., De Roo, F., Diaz-Pines, E., Haas, E., Hagen, M., Hajnsek, I., Jacobeit, J., Jagdhuber, T., Kalthoff, N., Kiese, R., Kunstmann, H., Kosak, O., Krieg, R., Malchow, C., Mauder, M., Merz, R., Notarnicola, C., Philipp, A., Reif, W., Reineke, S.,

Rödiger, T., Ruehr, N., Schäfer, K., Schrön, M., Senatore, A., Shupe, H., Völksch, I., Wanninger, C., Zacharias, S., and Schmid, H.P.: The SCALEX Campaign: Scale-Crossing Land Surface and Boundary Layer Processes in the TERENO-preAlpine Observatory, Bull. Am. Meteorol. Soc., 1217-1234, 2017.

Wunch, D., Wennberg, P.O., Toon, G.C., Keppel-Aleks, G., and Yavin, Y.G.: Emissions of greenhouse gases from a North American megacity. Geophysical Research Letters. 36, 2009.

Yu, J., Xie, Z., Sun, L, Kang, H., He, P., and Xing, G.: δ^{13}C-CH$_4$ reveals CH$_4$ variations over oceans from mid-latitudes to the Arctic, Scientific Reports, 5:13760, doi:10.1038/srep13760, 2015.

Zak, D., Reuter, H., Augustin, J., Shatwell, T., Barth, M., Gelbrecht, J., and McInnes, R.J.: Changes of the CO$_2$ and CH$_4$ production potential of rewetted fens in the perspective of temporal vegetation shifts.

Zerbe, S., Steffenhagen, P., Parakenings, K., Timmermann, T., Frick, A., Gelbrecht, J., and Zak, D.: Ecosystem Service Restoration after 10 Years of Rewetting Peatlands in NE Germany, Environmental Management, 51, 1194-1209, 2013.

Figure 1. The quadrocopter ALICE during take-off in Zarnekow on 5 September 2018.
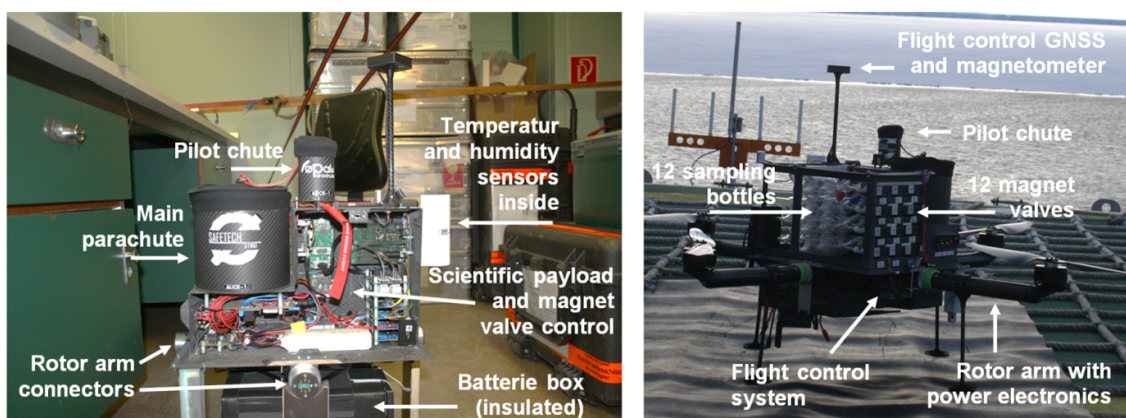
Figure 2. ALICE vital components.
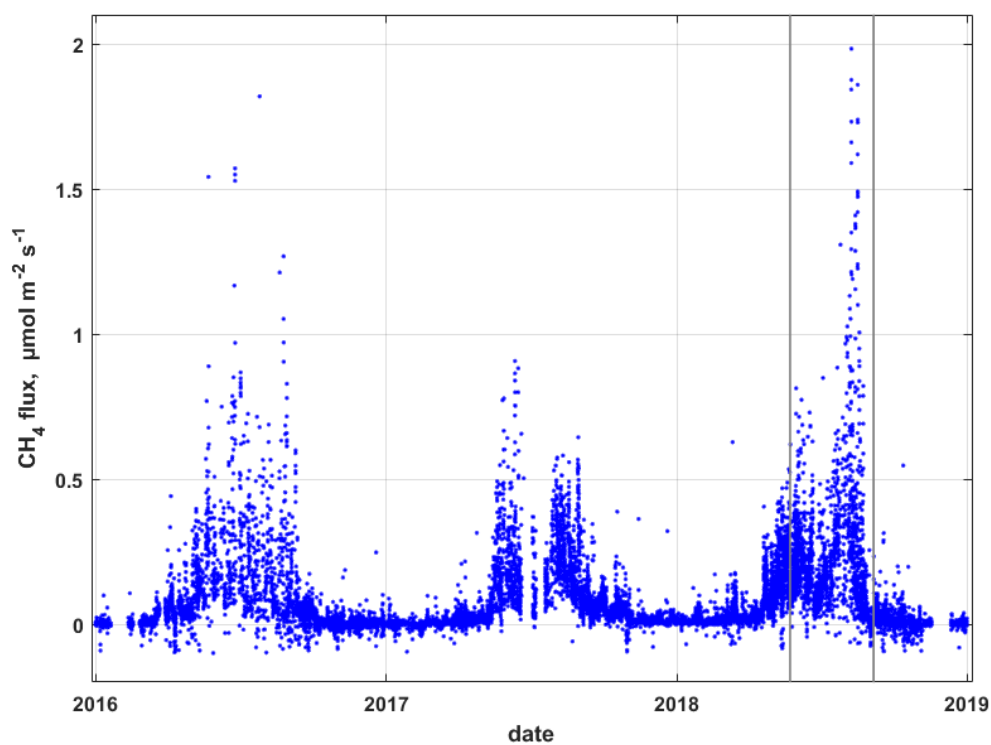
Figure 3. Methane fluxes at polder Zarnekow for the years 2016-2018. Indicated as vertical lines are the two measurement days, 23 May 2018 and 5 September 2018.
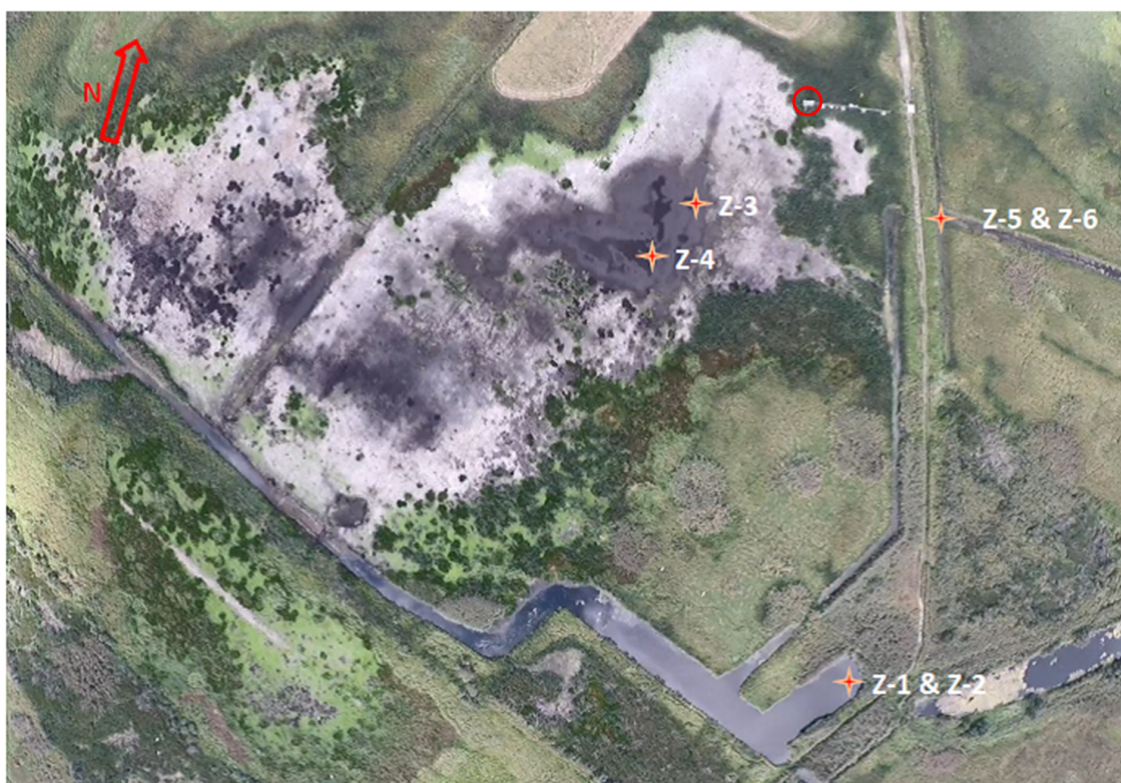
Figure 4. Aerial picture of the polder Zarnekow obtained with the quadrocopter ALICE on 5 September 2018. Almost the whole polder fell dry after the extremely warm and dry summer 2018. The sites where water samples were taken are indicated with Z1 to Z6. The location of the EC station is indicated with a red circle.
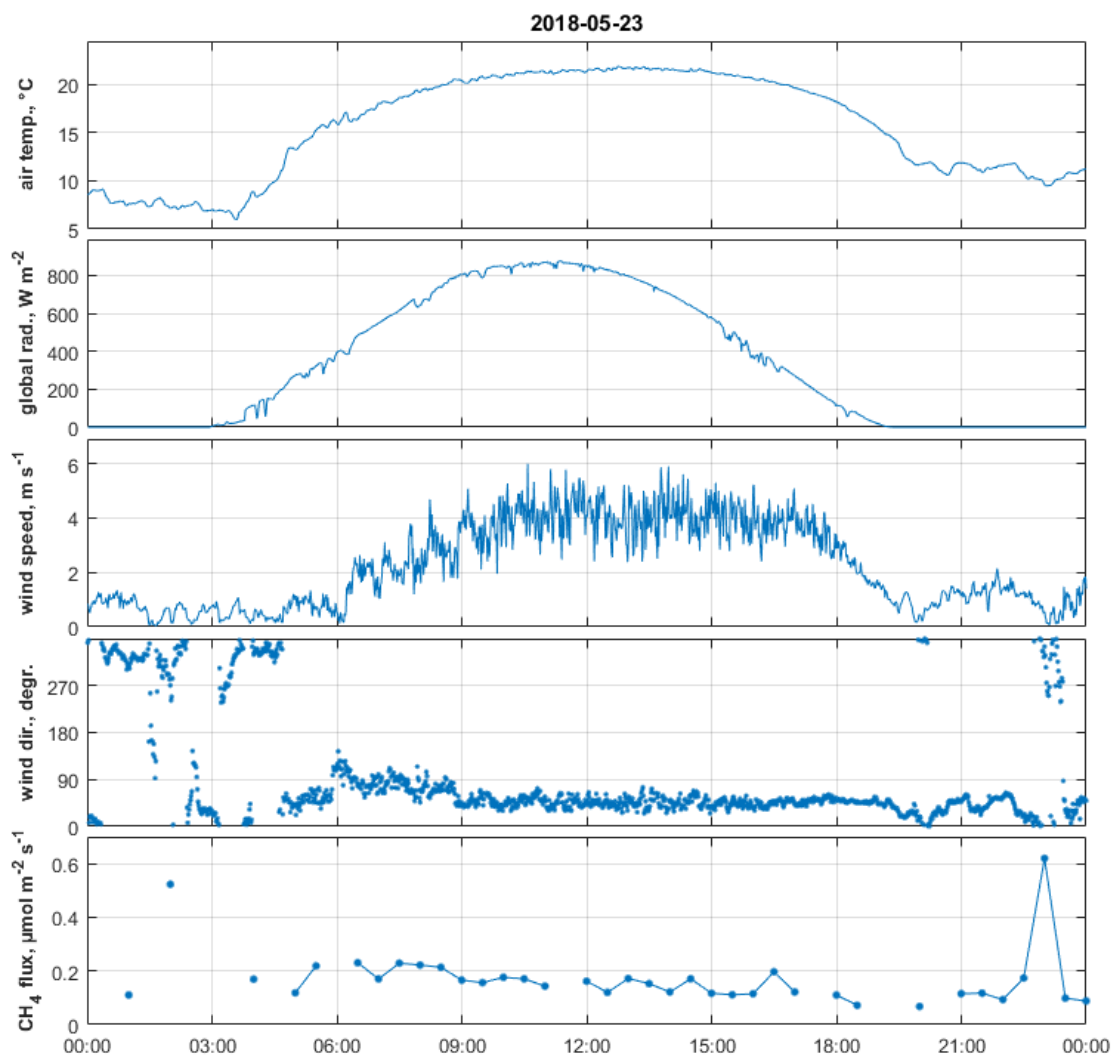
Figure 5. Diurnal course of the main meteorological parameters air temperature, global radiation, wind speed, wind direction, and methane flux recorded at the meteorological mast at Zarnekow on 23 May 2018.
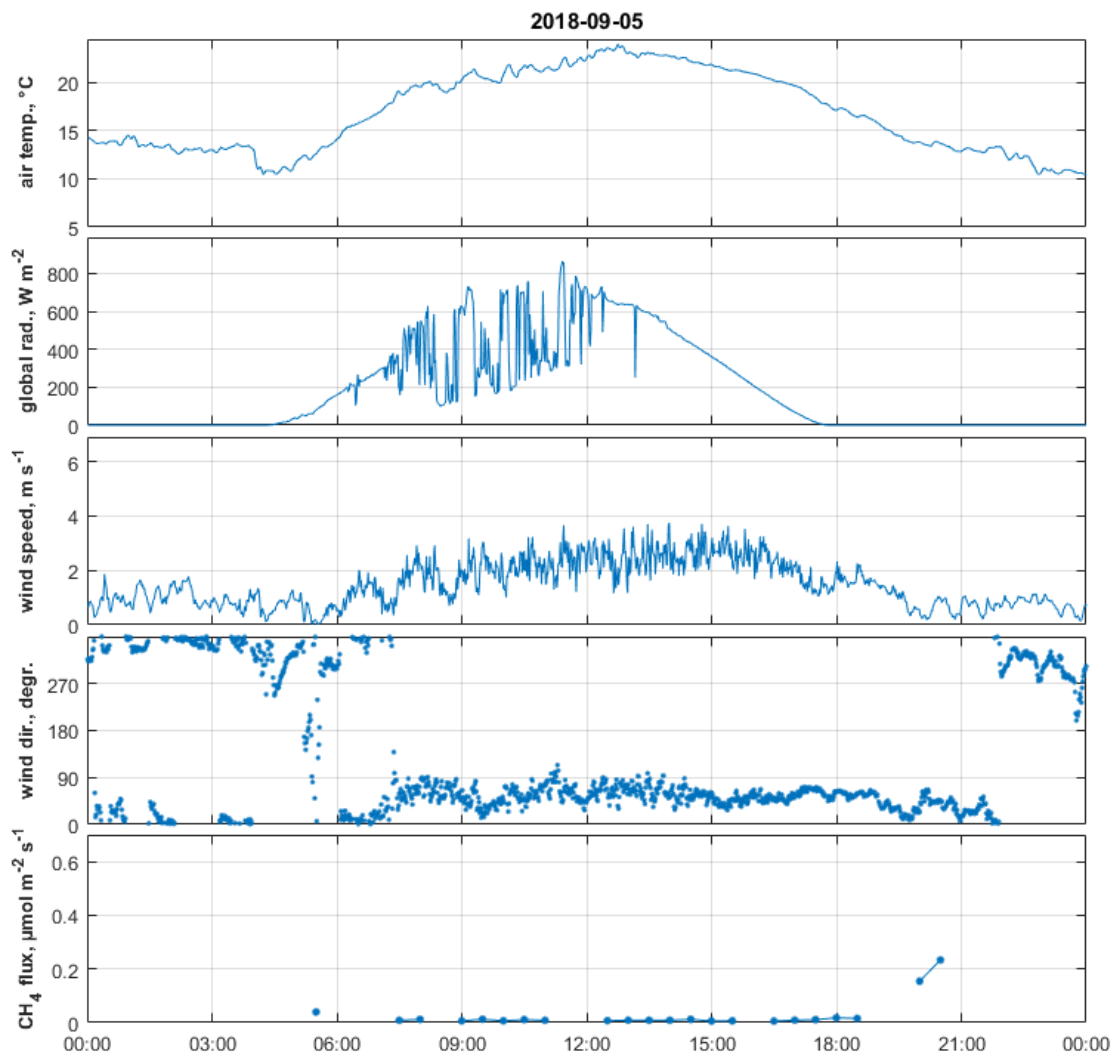
Figure 6. Diurnal course of the main meteorological parameters air temperature, global radiation, wind speed, wind direction, and methane flux recorded at the meteorological mast at Zarnekow on 05 September 2018.
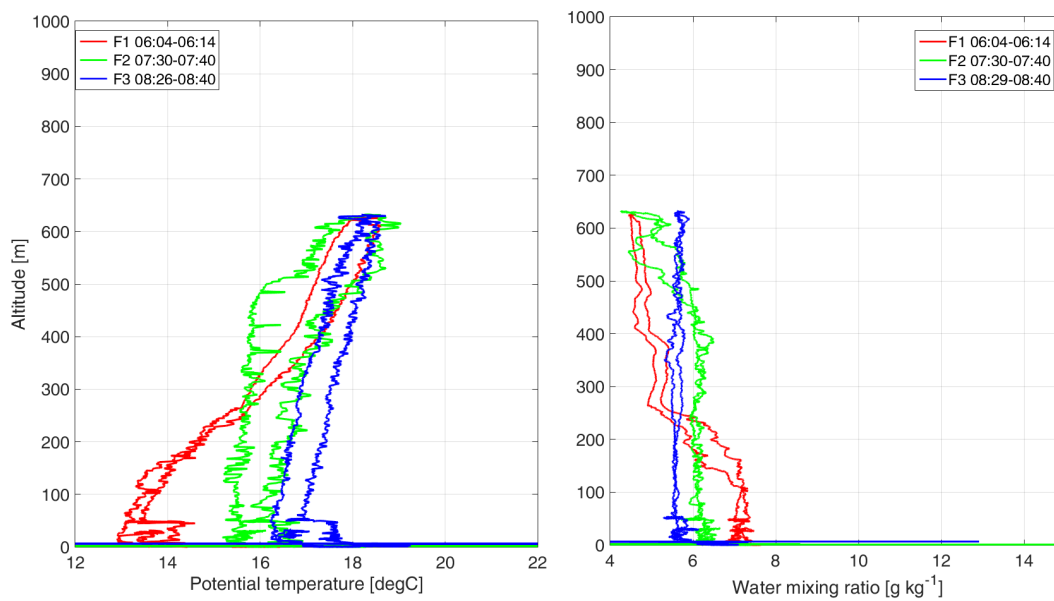
Figure 7. Profiles of potential temperature and water vapour mixing ratio obtained on 23 May 2018. The times of the five flights are given in UTC.
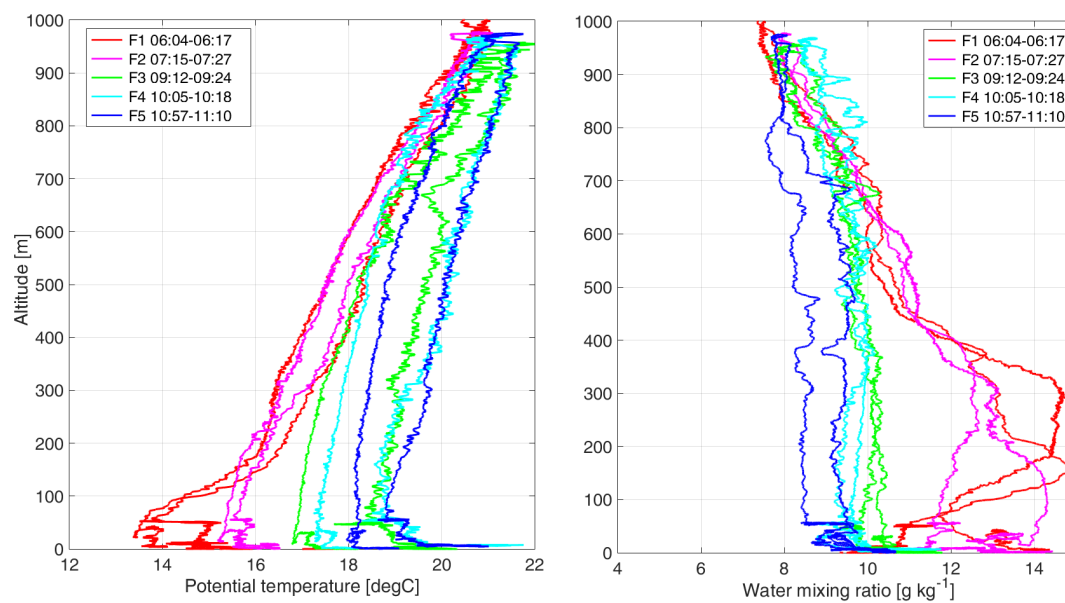
Figure 8. Profiles of potential temperature and water vapour mixing ratio obtained on 5 September 2018. The times of the three flights are given in UTC.
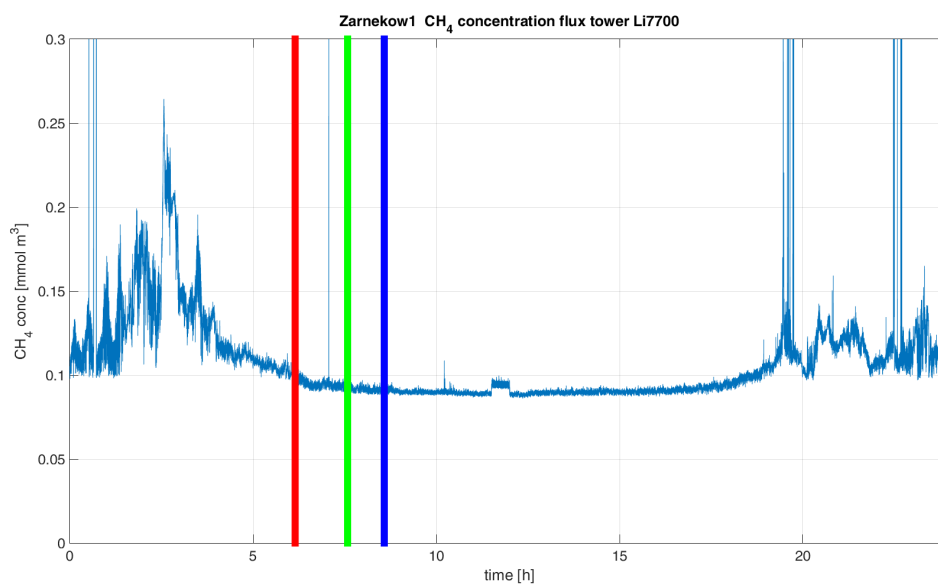
Figure 9. Continuous methane concentration recorded by the LI7700 sensor of the EC flux tower on 23 May 2018. The vertical bars represent the times of the quadrocopter flights, same colours as in Fig. 7.
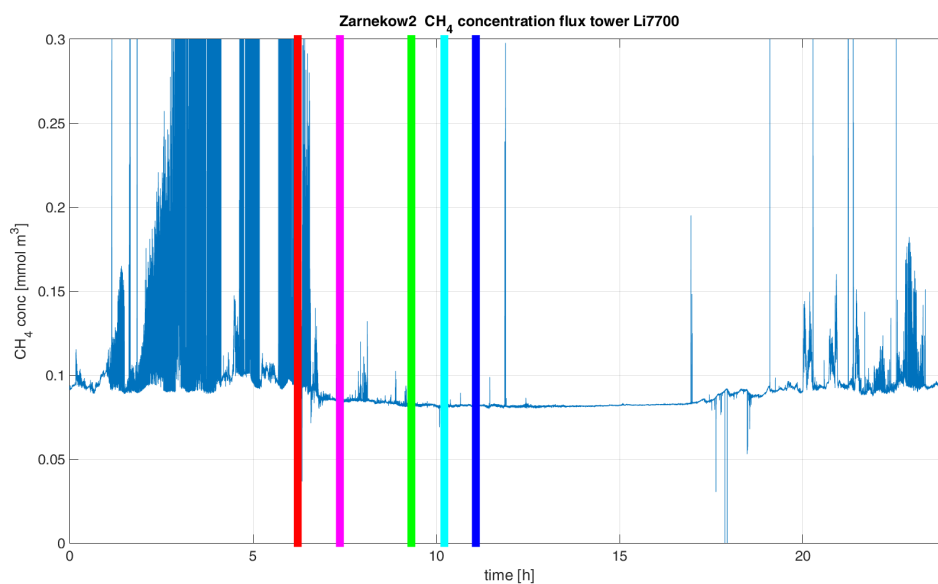
Figure 10. Continuous methane concentration recorded by the LI7700 sensor of the EC flux tower on 5 September 2018. The vertical bars represent the times of the quadrocopter flights, same colours as in Fig. 8.
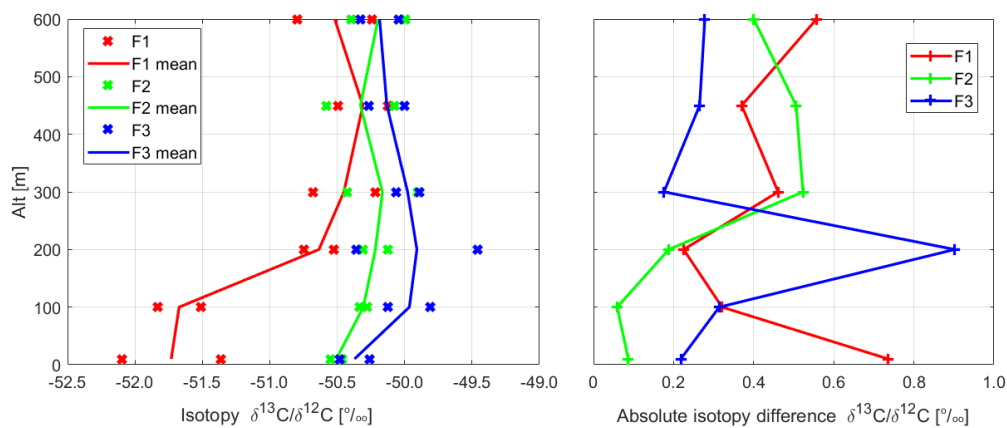
Figure 11. Profiles of a) $\delta^{13}C$ isotopy ratio for all air samples during the flights on 23 May 2018, and b) isotopy difference between the double samples filled simultaneously at the same altitude.
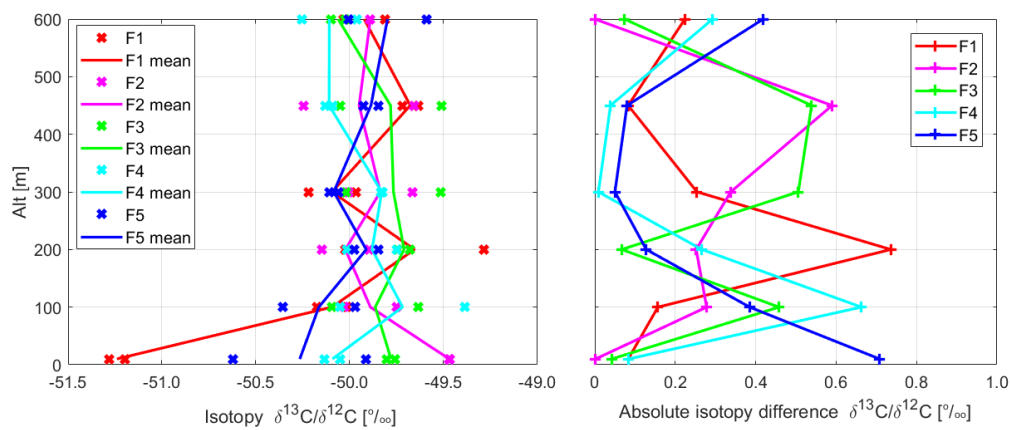
Figure 12. Profiles of a) $\delta^{13}C$ isotopy ratio for all air samples during the flights on 5 September 2018, and b) isotopy difference between the double samples filled simultaneously at the same altitude.
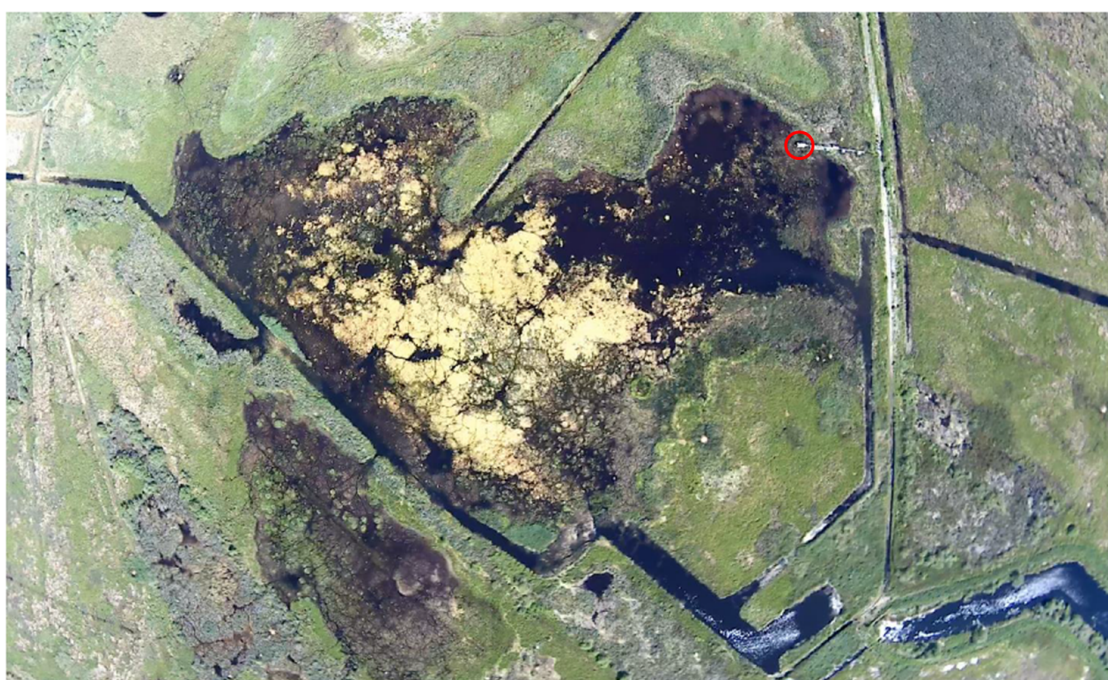
Figure 13. Aerial picture of the polder Zarnekow obtained with the quadrocopter ALICE on 23 May 2018. The location of the EC station is indicated with a red circle.
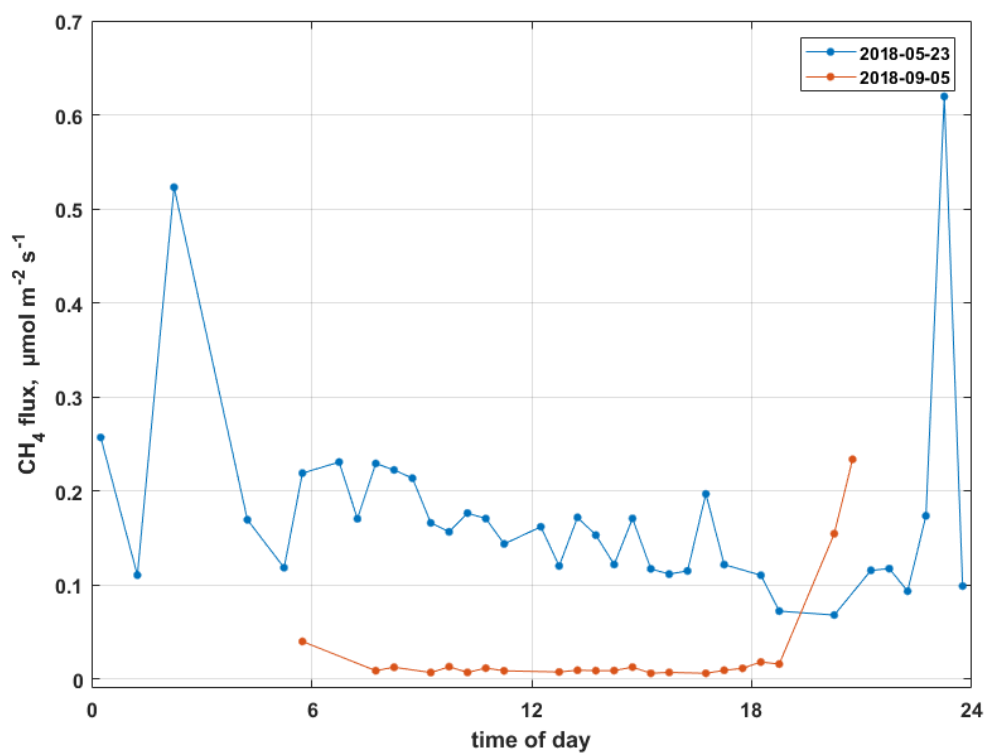
Figure 14. Methane fluxes during the two measurement days, 23 May and 5 September 2018.

Table 1. Water samples on 5 September 2018.

Number	location	water depth	colour	concentration [ppm]	isotopic ratio [‰]
Z-1	Peene River influx, surface water, 2 m from shore	5-10 cm	middle yellow	0.339	-30.5
Z-2	Peene River influx, deep water, 2 m from shore	40-50 cm	middle yellow	0.246	-30.1
Z-3	Polder Zarnekow, surface water, pond, 30 cm from edge	less than 5 cm	strong yellow	2312.7	-42.8
Z-4	Polder Zarnekow, surface water, pond	5-10 cm	strong yellow	4765.2	-48.2
Z-5	Trench in the East, 1 m from shore, between plants	5-10 cm	light yellow	111.38	-5.1
Z-6	Trench in the East, near shore	5-10 cm	light yellow	2397.9	-49.2